An Acad Bras Cienc (2022) 94(Suppl. 1): e20210432 DOI 10.1590/0001-3765202220210432
Anais da Academia Brasileira de Ciências | *Annals of the Brazilian Academy of Sciences*
Printed ISSN 0001-3765 I Online ISSN 1678-2690
www.scielo.br/aabc | www.fb.com/aabcjournal

GEOSCIENCES

Atmospheric blockings in Coupled Model Intercomparison Project Phase 5 models with different representations of Antarctic sea ice extent

CAMILA B. CARPENEDO & TÉRCIO AMBRIZZI

Abstract: This study investigated whether there are differences in the frequency and position of Southern Hemisphere atmospheric blockings between Coupled Model Intercomparison Project Phase 5 models with different representations of Antarctic sea ice extent in historical experiments. In the model with the greatest sea ice underestimation (Model for Interdisciplinary Research on Climate version 5) there is a weakening of the polar jet and an increase in 500-hPa height. These atmospheric conditions favor the predomination of simulated blocking frequency overestimations (autumn-winter), in relation to the observed (ERA-Interim). On the other hand, in the models with the greatest sea ice overestimations (Community Climate System Model version 4) and the better sea ice representation (Norwegian Earth System Model version 1) there is a strengthening of the polar jet and weaker positive differences in 500-hPa height in the Antarctic region. These atmospheric conditions favor a predominance of simulated blocking frequency underestimations (all seasons). All models present a good representation of the preferred blocking regions (South Pacific), although they do not represent the longitudinal location of the maximum frequency. In years of sea ice retraction (expansion), there is a predominance of a higher (lower) blocking frequency in the 60°S for all models and observed data.

Key words: Atmospheric blockings, sea ice, CMIP5, Antarctica.

INTRODUCTION

Prolonged episodes of extreme weather conditions such as droughts/floods (e.g., Trenberth & Guillemot 1995, Mo et al. 1997, Rodrigues & Woollings 2017) and heatwaves (e.g., Kalkstein et al. 1996, Karl & Knight 1997, Rodrigues & Woollings 2017) are often associated with periodic atmospheric flow anomalies (Dole 1986a, b, Higgins & Schubert 1994, 1996), which can last from a few days to weeks. Among these phenomena, atmospheric blockings are associated with extreme weather events due to their systematic and persistent nature, affecting the normal propagation of transient systems. A better understanding of the mechanisms that originate, maintain and dissipate such phenomena is of great importance for the success of short, mid- and long term predictions, considering that atmospheric blockings play an important role in atmospheric variability in various time scales (e.g., Rex 1950, Tsou & Smith 1990, Nakamura & Wallace 1993, Nakamura 1994, Nakamura et al. 1997, Lupo & Smith 1998, Luo et al. 2002, Nakamura & Fukamachi 2004, Tyrlis & Hoskins 2008, Rodrigues & Woollings 2017).

Among the mechanisms associated with atmospheric blockings, in the Northern Hemisphere orographic forcing is dominant

(Kikuchi 1969, Shabbar et al. 2001), while in the Southern Hemisphere, due to the lower orography asymmetry, the main mechanism is thermal forcing (Coughlan 1983, Ambrizzi et al. 2009). The location of sea surface temperature (SST) anomalies in relation to large-scale flow is one of the conditions for these anomalies to produce changes in atmospheric circulation (Shukla 1986, Kidston et al. 2011, Raphael et al. 2011). There is a great potential for Antarctic sea ice to affect atmospheric circulation, from the surface to mid-troposphere levels, as the pack ice edge is in a very sensitive region - south of the Southern Hemisphere baroclinic zone (Raphael et al. 2011, Kidston et al. 2011, Parise et al. 2015). Kidston et al. (2011) showed that southern mid-latitude positive SST anomalies of 0.5 to 1.0°C resulted in surface heat flux anomalies of 1 to 5 Wm^{-2}, while Antarctic sea ice extent (SIE) anomalies generated flux anomalies greater than 100 Wm^{-2}. The authors thus conclude that variations in SIE have the potential to exert more significant influence on atmospheric circulation than SST anomalies.

Although the relationship between atmospheric blockings and SIE is still not well known (e.g., Washington & Meehl 1984, Bates & Meehl 1986, Liu et al. 2012, Tang et al. 2013, Luo et al. 2018), there is evidence that it exists. Southern Hemisphere atmospheric blockings mainly occur between the 50° and 65°S latitudes (Sinclair 1996, Mendes et al. 2008), so atmospheric blockings located at higher latitudes are more persistent than those over lower latitudes (Oliveira et al. 2014). In addition, the highest frequency of atmospheric blockings occur in the cold season (Van Loon 1956, Mendes et al. 2008, Oliveira & Ambrizzi 2016), which coincides with the maximum Antarctic SIE.

Washington & Meehl (1984) and Bates & Meehl (1986) analyzed the effect of an atmosphere with twice the CO2 concentration in the Southern Hemisphere atmospheric blocking frequency. The authors concluded that, as the tropospheric temperature increases, there is an increase in the 500 hPa geopotential height, near the region where sea ice retracts and the atmospheric blocking frequency is reduced. On the other hand, previous studies have suggested that Arctic warming and sea ice loss led to an increase in the occurrence and persistence of blocking events in the Northern Hemisphere (e.g., Liu et al. 2012, Tang et al. 2013, Luo et al. 2018). The authors justified that the weakening of the westerly winds tend to amplify the ridges and troughs, which are susceptible to the formation of atmospheric blockings related circulations (Liu et al. 2012).

The Antarctic SIE has shown an increasing trend in the last decades (1979-2014), followed by an abrupt reduction (2014-2017), greater than the loss of the Arctic SIE in the last three decades (Parkinson 2019). In the Coupled Model Intercomparison Project Phase 5 (CMIP5) models, produced by the Intergovernmental Panel on Climate Change (IPCC), the representation of the Antarctic SIE shows improvements in relation to CMIP3 (IPCC 2013). Despite this, considering four decades of satellite measurements, most CMIP5 models show a negative trend in Antarctic SIE, contrasting with the observed positive trend (Turner et al. 2013, Parkinson 2019). Internal variability (Landrum et al. 2012, Polvani & Smith 2013, Zunz et al. 2013); model sensitivity to warming (Rosenblum & Eisenman 2017); problems in simulating high latitude winds (Koldunov et al. 2010) and ocean heat advection and mixing (Melsom et al. 2009) contribute to these uncertainties. The rare CMIP5 models, with a positive trend of the Antarctic SIE overestimate the interannual variability, resulting in a large range of possible trends, masking the differences between the models and observations (Zunz et al. 2013).

The objective of this study was to investigate whether there are differences in the frequency and position of the Southern Hemisphere atmospheric blockings, between CMIP5 models with different representations of Antarctic SIE produced by historical experiments. The results may further the understanding of the mechanisms related to Southern Hemisphere atmospheric blockings, and this in turn may improve mid- and long-term forecasting of these systems.

MATERIALS AND METHODS

Data

We used three atmosphere-ocean general circulation models (AOGCM) from the Working Group on Coupled Modeling/ World Climate Research Program, comprising CMIP5 (Taylor et al. 2012), employed as a basis for the IPCC Fifth Assessment Report. Three AOGCM were chosen for their distinctive Antarctic SIE representations, in terms of greatest underestimation, the best representation and greatest overestimation. The MIROC5 (Model for Interdisciplinary Research on Climate version 5) is the one with the highest underestimation for Antarctic SIE, the NorESM1-M (Norwegian Earth System Model version 1) presents the best representation and the CCSM4 (Community Climate System Model version 4) presents the highest overestimation (Turner et al. 2013). For selected models, we have obtained the daily historical simulations (1979-2005) of sea ice concentration (%), 500-hPa geopotential height (m) and 250-hPa zonal wind (ms^{-1}).

MIROC5 - a joint effort of the Atmosphere and Ocean Research Institute (The University of Tokyo); the National Institute for Environmental Studies and the Japan Agency for Marine-Earth Science and Technology - is an AOGCM with atmospheric, oceanic, sea ice and land components (Watanabe et al. 2010). The sea ice component calculates the evolution of thickness distribution on a subgrade scale, following the governing equations of Thorndike et al. (1975). In each horizontal grid, sea ice is divided into five categories, plus open water. The thermal capacity of sea ice is considered in the module. Salinity is fixed at 5 psu. Sea-ice albedo, at 0°C, is 0.8 (visible band) and 0.65 (near infrared band), while at less than -5°C, it is 0.9 (visible band) and 0.8 (near infrared band) (Watanabe et al. 2010). Detail of other components can be seen in Watanabe et al. (2010).

The CCSM4, offered by the National Center for Atmospheric Research (NCAR), is an AOGCM with atmospheric, oceanic, sea ice and land components, which are connected by a coupler that exchanges state and flow information between the components (Gent et al. 2011). The sea ice component is based on the Community Ice Code (CICE) version4, which includes a delta-Eddington radiative transfer scheme, using inherent optical properties to define dispersion and absorption characteristics of snow and sea ice, including absorbers such as black carbon and dust (Gent et al. 2011). The other components can be seen in detail in Gent et al. (2011).

The NorESM1-M was developed by the Norwegian Climate Center (NCC) and is largely based on the CCSM4 model. The main differences are (Bentsen et al. 2013): (1) the isopycnic coordinate ocean module; (2) the CAM4 atmospheric module is replaced by the CAM4-Oslo, with aerosol parameterizations, aerosol-cloud interactions and aerosol-radiation. The finite volume dynamical core has a horizontal resolution of 1.9° x 2.5°, model top at 2.917 hPa, 26 vertical levels and hybrid sigma-pressure co-ordinate. The grid mesh size is double that of the standard version used in CCSM4; (3) Sea ice and land modules are basically the same as CCSM4 except that mineral dust aerosols on snow and

sea ice are based on the aerosol calculations in CAM4-Oslo.

Here we focus on the period 1979-2005 since this period overlaps with the available satellite record of SIE, which was obtained from the National Snow and Ice Data Center, derived from the National Aeronautics and Space Administration (NASA) team algorithm (ftp://sidads.colorado.edu/DATASETS/NOAA/G02135/).

To identify atmospheric blocking events and to compare AOGCM historical simulations and climate reanalysis we used the 6-hourly atmospheric fields, relative to 500-hPa geopotential height (m) and 250-hPa zonal wind (ms^{-1}), of the ERA-Interim reanalysis (ECMWF Data Server, 1.5° x 1.5°), from 1979 to 2005.

Blocking index

The blocking index used here is an adapted version of the objective method by Tibaldi et al. (1994), according to Oliveira et al. (2014). The adaptations to the original blocking index were adjusted to a smaller horizontal spacing of the ERA-Interim reanalysis (1.5° x 1.5° rather than 3.75° x 3.75° used in the original method) and stratified into two latitude bands, which are 48° ± ΔERA and 60°S ± ΔERA (ΔERA = 1.5°, 3°, 4.5° and 6° latitude). Thus, it is possible to analyze the latitudinal variation of atmospheric blocking events by comparing the latitude bands (Oliveira et al. 2014). The Geopotential Height Gradient North (GHGN) and South (GHGS), which are simultaneously calculated for all longitudes per latitude band, using 500-hPa geopotential height, give the blocking index. Flow is defined as blocked when the conditions of GHGN being greater than 0 m $°lat^{-1}$ and GHGS being less than 10 m $°lat^{-1}$ are simultaneously satisfied for at least one latitude delta ($\Delta\varphi$ = 1.5°, which is the spatial resolution of the ERA-Interim reanalysis) and for at least 15° longitude (1100 km at medium latitudes). This extension criterion is sufficient for an atmospheric blocking event pattern (e.g., Verdecchia et al. 1996, Tibaldi et al. 1997, Barriopedro et al. 2006, Oliveira & Ambrizzi 2016). GHGN can be interpreted as the geopotential height gradient or atmospheric blocking intensity. GHGS is the geopotential height gradient at high latitudes. This condition was imposed by Tibaldi et al. (1994) to prevent detached cold cutoff lows, anomalously located at polar latitudes, from being misidentified as atmospheric blocking events, as they can also result in negative values (Lejeñas 1984). A time constraint was also applied. For an episode to be characterized as an atmospheric blocking event, it must persist for at least 3 days, hereafter called the atmospheric blocking event (Sinclair 1996, Marques & Rao 1999, Oliveira et al. 2014). Atmospheric blocking events are presented here in the form of seasonal frequency of days with atmospheric blocking events by longitude (%), according to previous studies (e.g., Marques & Rao 1999, Mendes et al. 2008, Oliveira & Ambrizzi 2016, and references therein).

Methods

Initially, the daily AOGCM simulations were interpolated with the same resolution as the ERA-Interim reanalysis (1.5° x 1.5°), for later comparison between the data sets. Season definition was performed according to Zwally et al. (2002), focusing on studies involving sea ice cover: summer (January, February and March), autumn (April, May and June), winter (July, August and September) and spring (October, November and December).

Simulated SIE was computed as the total area of all grid cells where sea ice concentration was greater than 15%. Annual cycle, mean annual/ seasonal and standard deviation of SIE of each model was compared in relation to the SIE observed in the satellite data. Finally, we compared the frequency of blocking events

in years of negative (retraction) and positive (expansion) anomalies of Antarctic SIE for all models and satellite data/ climate reanalysis.

To assess the AOGCM potential for simulating atmospheric blockings, in historical experiments, this study initially compared the seasonal frequency and the position of the simulated atmospheric blocking events to the climate reanalysis, in each selected model. To study atmospheric blockings, it is necessary that some atmospheric variables be well represented in the AOGCM, such as the 500-hPa geopotential height and the high-level zonal wind. Thus, the spatial pattern of these simulated atmospheric fields were compared with climate reanalysis through spatial difference analysis. We also analyzed the standard deviation of the simulated atmospheric fields to assess the variability of 500-hPa geopotential height and 250-hPa zonal wind.

RESULTS

Assessment of Antarctic sea ice extent in the CMIP5 models

Figure 1 shows the mean annual cycle (1979-2005) of the Antarctic SIE, from satellite and simulated data. We can observe that all models represent the annual cycle of the Antarctic SIE relatively well, with a minimum of 3.1 × 10^6 km² in February and a maximum of 18.4 × 10^6 km² in September (Figure 1, black line). MIROC5 is the model with the greatest underestimation of the mean annual cycle of the Antarctic SIE (Figure 1, gray dotted line), with a minimum of 0.2 × 10^6 km² (February) and a maximum of 8.6 × 10^6 km² (September). Furthermore, MIROC5 is the model with the lowest annual (4.3 ± 3.2 × 10^6 km²) and seasonal (ranging from 0.4 ± 0.1 × 10^6 km² in summer to 7.8 ± 0.6 × 10^6 km² in winter) SIE (Table I). On the other hand, CCSM4 is the model with the highest overestimation of the mean annual cycle of SIE, with a minimum of 9.7 × 10^6 km² (March) and a maximum of 21.9 × 10^6 km² (September) (Figure 1, gray line). The annual SIE is 17.4 ± 4.3 × 10^6 km², ranging from

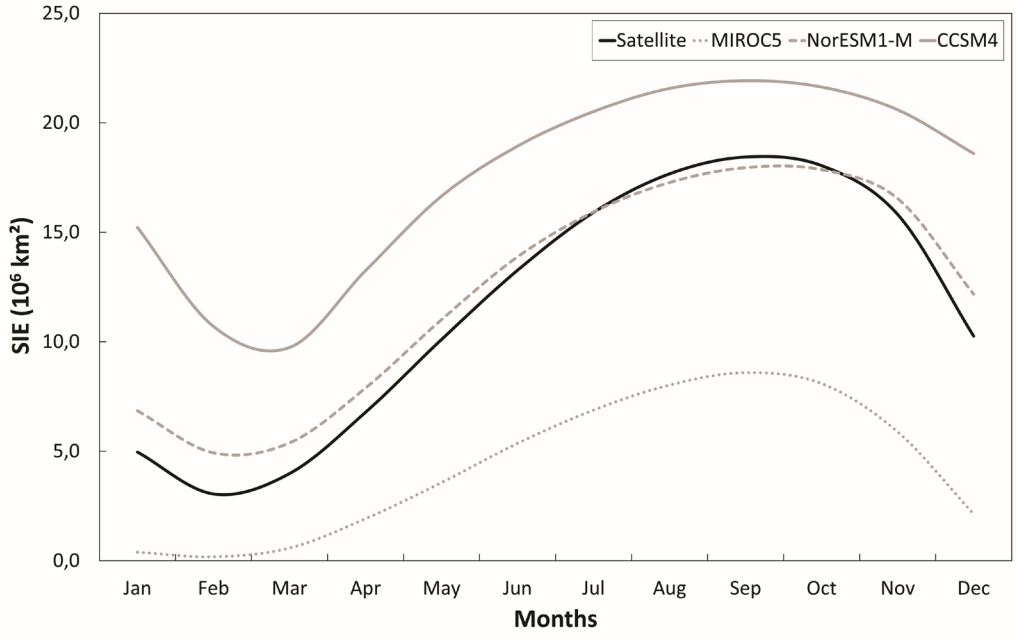

Figure 1. Mean annual cycle (1979-2005) of Antarctica SIE derived from satellite data and simulated in the 3 CMIP5 models (MIROC5, NorESM1-M e CCSM4).

11.9 ± 0.7 × 10^6 km² in summer to 21.3 ± 0.6 × 10^6 km² in winter (Table I). NorESM1-M is the model that best represents the mean annual cycle of the Antarctic SIE, with a minimum of 4.9 × 10^6 km² (February) and a maximum of 17.9 × 10^6 km² (September) (Figure 1, gray dashed line). However, overestimation prevails throughout the year, with the exception of August to October, when there is an underestimation of the SIE. This fact can also be observed through the annual (12.3 ± 5.0 × 10^6 km²) and seasonal (varying between 5.7 ± 0.5 × 10^6 km² in summer and 17.0 ± 0.4 × 10^6 km² in winter) SIE (Table I). These results are in agreement with Turner et al. (2013).

MIROC5

The preferred atmospheric blocking regions in the MIROC5 historical experiment (Figure 2) - the AOGCM with the greatest Antarctic SIE underestimation (Turner et al. 2013) - are relatively well represented in the Southern Hemisphere, with preferential location over the South Pacific. These findings have also been observed by Van Loon (1956), Lejeñas (1984), Trenberth & Mo (1985), Tibaldi et al. (1994) and Oliveira et al. (2014). However, there is a shift to the west of the maximum frequency of blocking events in the 48°S latitude band in winter (from ~170°W to ~160°E; Figure 2c), and in the 60°S latitude band in autumn (from ~95°W to ~150°W; Figure 2b), winter (from ~110°W to ~135°W) and spring (from ~100°W to 160°W; Figure 2d). There is an eastward shift in the 48°S latitude band in summer (from ~170° to ~160°W; Figure 2a), autumn (from ~175° to ~155°W; Figure 2b) and spring (from ~165°W to ~110°W). There is a predomanace of overestimation in the frequency of blocking events at 48°S (autumn and winter) and 60°S (winter and spring) latitude bands, reaching a 260% increase in ~160°E (from 2% of the observed frequency to 7.2% of the simulated frequency) in the 48°S band during winter. In summer (48°S and 60°S bands), autumn (60°S band) and spring (48°S band) there is an underestimation in frequency of blocking events, reaching a reduction of ~93% in ~180° (from ~4.1% of the observed frequency to 0.3% of the simulated frequency) in the 48°S band during summer.

In Figure 3 we present the 500-hPa geopotential height and the 250-hPa zonal wind seasonal differences, between the MIROC5 historical experiments and the climate reanalysis. The 500-hPa geopotential height is overestimated by the MIROC5 throughout the Southern Hemisphere and in all seasons (Figures 3a-d), with greater differences south of 40-50°S and in winter. The greatest 500-hPa geopotential height variability occurs in the South Pacific in all seasons (Figures 3e-h), with higher standard deviations in cold seasons.

The 250-hPa zonal wind difference, between the simulated and the climate reanalysis, shows a weakening of the polar jet in all seasons (Figures 3i-l), with greater differences in winter

Table I. Annual and seasonal mean (1979-2005), with respective standard deviations, of the Antarctic SIE derived from satellite data and simulated in the 3 CMIP5 models (MIROC5, NorESM1-M and CCSM4).

	Satellite	MIROC5	NorESM1-M	CCSM4
Annual	11.5 ± 5.8	4.3 ± 3.2	12.3 ± 5.0	17.4 ± 4.3
Summer	4.0 ± 0.4	0.4 ± 0.1	5.7 ± 0.5	11.9 ± 0.7
Autumn	10.1 ± 0.5	3.6 ± 0.4	10.9 ± 0.4	16.3 ± 0.6
Winter	17.3 ± 0.3	7.8 ± 0.6	17.0 ± 0.4	21.3 ± 0.6
Spring	14.8 ± 0.5	5.4 ± 0.6	15.5 ± 0.6	20.3 ± 0.6

and smaller differences in summer. On the other hand, there is a strengthening of the subtropical jet in the north, which is more evident in winter. The highest zonal flow variability, at high levels, occurs between 20°S and 70°S in cold seasons (Figures 3n-o), while in warm seasons the maximum variability is restricted between 30°S and 60°S (Figures 3m, 3p). In winter, the cold fronts reach lower latitudes and the polar jet accompanies the displacement of these systems (Escobar 2009). In this way, the polar jet shows a greater asymmetry in cold seasons when compared to warm seasons (Trenberth 1991, Escobar 2009).

CCSM4

In the CCSM4, the AOGCMs with the highest overestimation of the Antarctic SIE (Turner et al. 2013), the preferred atmospheric blocking regions over the South Pacific, are relatively well simulated in all seasons (Figure 4). Despite this, there is an eastward shift of the maximum frequency of blocking events in the 48°S latitude band during summer (from ~170° to ~160°W; Figure 4a), autumn (from ~175°W to ~160°W; Figure 4b), winter (from 165°W to 140°W; Figure 4c) and spring (from 165°W to 150°W; Figure 4d), while the displacement is westward in the 60°S latitude band in summer (from ~155°W to 160°W) and winter (from ~110°W to ~135°W). In general, the frequency of blocking events in the 48°S and 60°S latitude bands is underestimated by the CCSM4 in all seasons, mainly in the South Pacific. The highest differences between the simulated and the climate reanalysis occur in winter, with reduction of up to 65% in ~165°W (from 6% of the climate reanalysis frequency

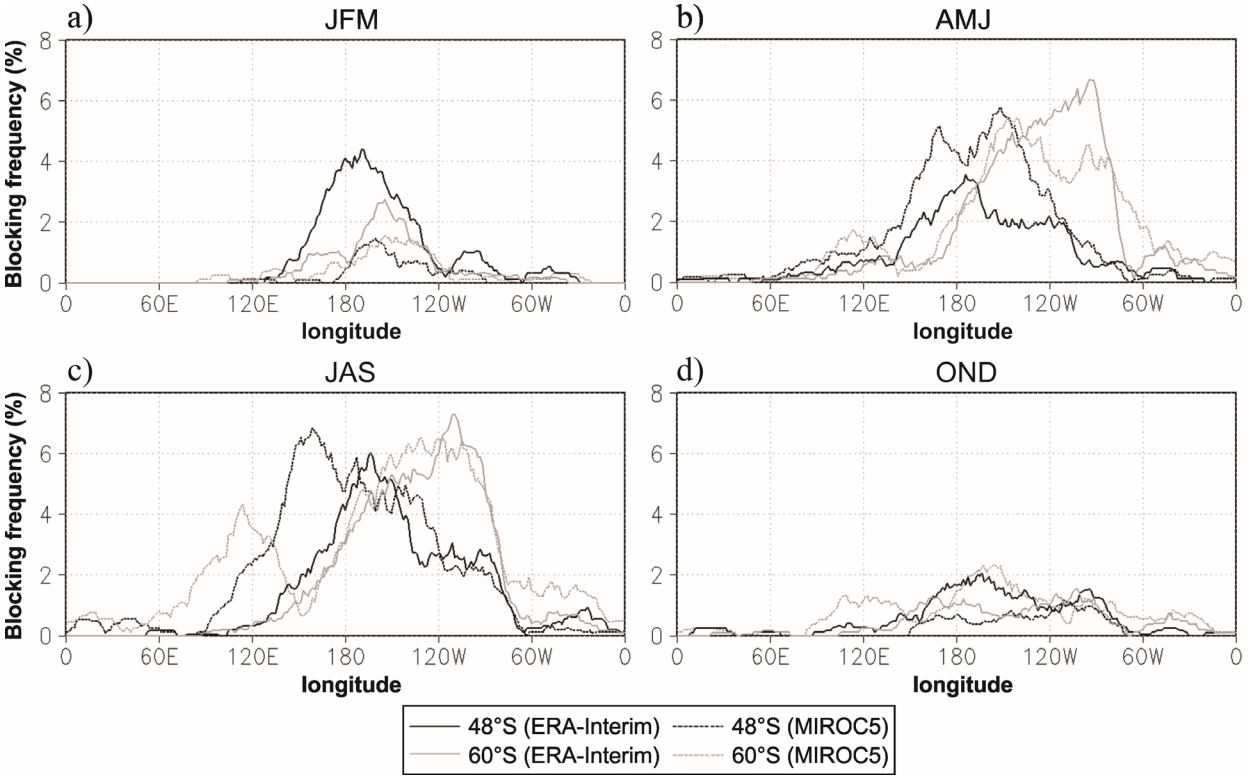

Figure 2. Seasonal frequency of blocking events by longitude (%) in the ERA-Interim reanalysis (continuous lines) and in the MIROC5 historical experiment (dashed lines) during (a) summer (JFM), (b) autumn (AMJ), (c) winter (JAS) and (d) spring (OND) over 1979-2005.

to 2.1% of the simulated frequency) in the 60°S band.

With relation to the 500-hPa geopotential height difference between the simulated and the climate reanalysis, there is a predominance of overestimation in all seasons and in practically the entire Southern Hemisphere (Figures 5a-d). In the Antarctic region we can observe the smallest differences, especially in the autumn and winter, reaching underestimation in autumn around 60°E and 120°W, in the Ross and Dumont D'Urville seas, and in winter around 60°W, on the Antarctic Peninsula and western Weddell Sea. In terms of standard deviation of the simulated 500-hPa geopotential height, the largest values are observed in autumn (Figure 5f), located in the mid- and high latitudes of the entire Southern Hemisphere. We can observe the same spatial pattern of standard deviation in other seasons (Figures 5e, 5g, 5h), with lower values during summer.

Through the 250-hPa zonal wind difference between the simulated and the climate reanalysis, we can detect a strengthening of the polar jet in all seasons (Figures 5i-l), with greater differences in the South Pacific and Indian Oceans. On the other hand, there is a weakening of the subtropical jet over Australia in all seasons, extending over the South Pacific, around 40°S. In tropical South America, there is a weakening of the subtropical jet and an apparent shift to the south. Among the seasons, winter is the one with the smallest differences between the simulated and the climate reanalysis (Figure 5k), while summer and autumn are the ones with the highest differences (Figures 5i-j). In relation

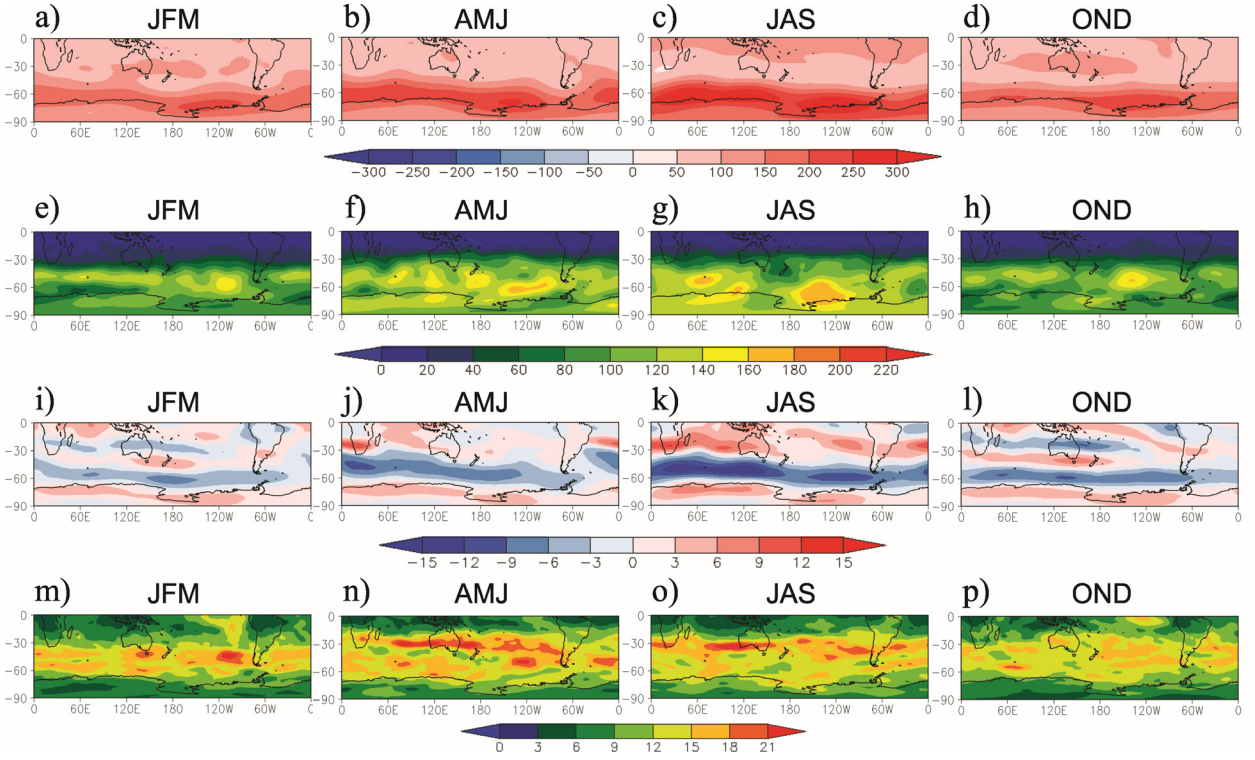

Figure 3. Seasonal difference of (a, b, c, d) 500-hPa geopotential height (m) and (i, j, k, l) 250-hPa zonal wind (ms^{-1}) between the MIROC5 historical experiment and the ERA-Interim reanalysis and standard deviation of (e, f, g, h) 500-hPa geopotential height (m) and (m, n, o, p) 250-hPa zonal wind (ms^{-1}) from the MIROC5 historical experiment during summer (JFM; first column), autumn (AMJ; second column), winter (JAS; third column) and spring (OND; fourth column) over 1979-2005.

to the standard deviation of the 250-hPa zonal wind simulated, in summer (Figure 5m) there is a smaller standard deviations in the Southern Hemisphere in relation to the other seasons. Spatially, autumn (Figure 5n) is the season with the highest standard deviation values, mainly over the South Pacific and Indian Oceans, in addition to the extratropical South America. In winter (Figure 5o) the highest standard deviation values occur in the region of the subtropical jet in the southern South America, the Indian and South Pacific Oceans. Finally, in spring (Figure 5p) we can observe the highest standard deviations in the region of the polar jet and the subtropical jet in the South Pacific and South Atlantic, with values of up to 18-21 ms^{-1}.

NorESM1-M

NorESM1-M, AOGCM that best represents Antarctic sea ice (Turner et al. 2013), represents relatively well the preferred regions of occurrence of the Southern Hemisphere atmospheric blockings (Figure 6). However, there is an eastward shift of the maximum frequency of blocking events in the 48°S latitude band in summer (from ~170°W to ~150°W; Figure 6a), autumn (from ~175°W to ~135°W ; Figure 6b), winter (from ~165°W to ~145°W; Figure 6c) and spring (from ~165°W to 120°W; Figure 6d), while in the 60°S latitude band the displacement is westward in autumn (from ~95°W to ~140°W) and winter (from ~110°W to ~120°W). There is a predominance of underestimation of the frequency of blocking events by the NorESM1-M model in all seasons and latitude bands, especially in summer, with a reduction of up to 90.9% at ~170°W (from 4.4%

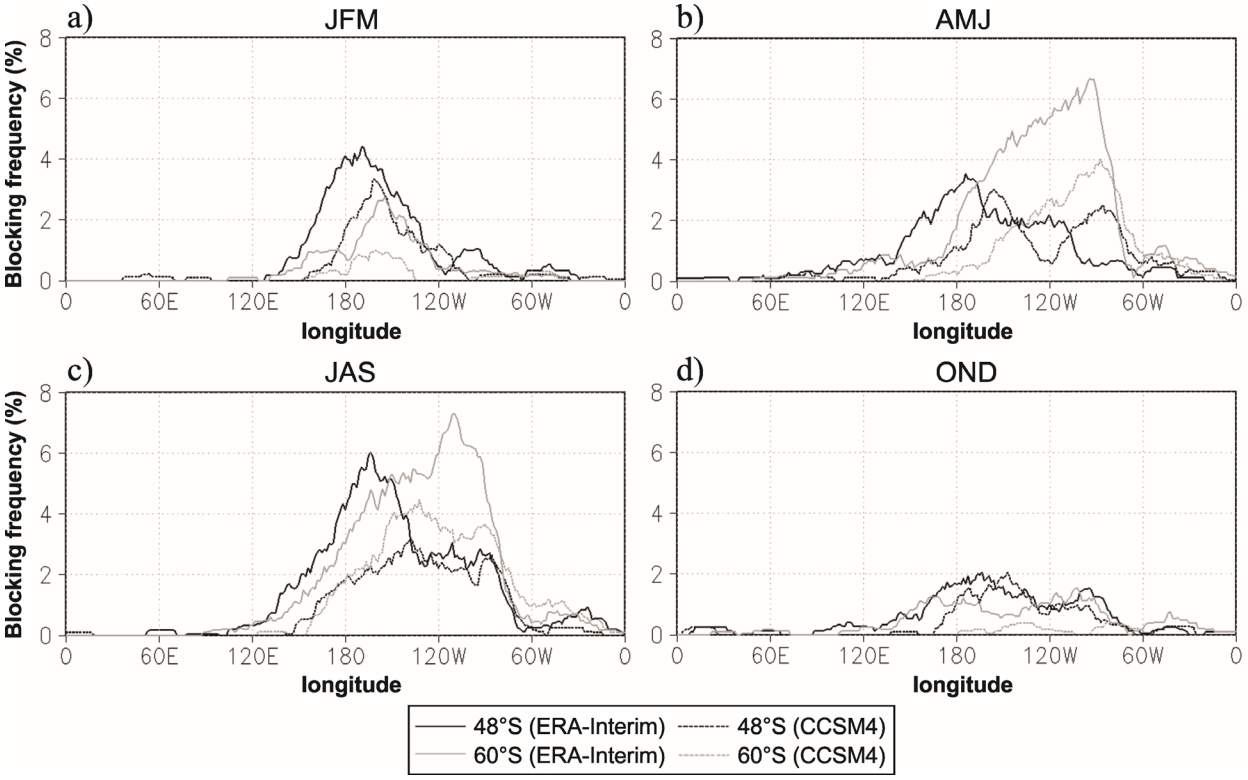

Figure 4. Seasonal frequency of blocking events by longitude (%) in the ERA-Interim reanalysis (continuous lines) and in the CCSM4 historical experiment (dashed lines) during (a) summer (JFM), (b) autumn (AMJ), (c) winter (JAS) and (d) spring (OND) over 1979-2005.

of frequency in the observed for 0.4% in the simulated) in the 48°S band.

The 500-hPa geopotential height difference fields show a predominance of overestimation in all seasons in the Southern Hemisphere (Figures 7a-d). The greatest differences are observed at mid-latitudes, with the most intense centers in the South Atlantic (summer), Indian Ocean (autumn) and South Pacific (winter). The greatest variability of the 500-hPa geopotential height occurs in the South Pacific, centered at ~120°W in the transition seasons (spring and autumn; Figures 7f, 7h) and at ~100°W in winter (Figure 7g).

Between summer and winter, there is a strengthening of the polar jet, more intense in the Indian Ocean during autumn, and a weakening of the subtropical jet to the north (Figures 7i-k). On the other hand, in spring there is a predominance of a slight weakening of the polar jet and a strengthening of the subtropical jet in the north, in the central-west of the South Pacific (Figures 7l). The greatest 250-hPa zonal wind variability occurs in the cold seasons (autumn and winter), with higher standard deviations between Australia and southern South America (Figures 7n-o).

Atmospheric blockings during Antarctic sea ice extent retraction and expansion

Figure 8 shows the seasonal frequency of blocking events, in the 48°S latitude band, in years of SIE Antarctic retraction and expansion (1979-2005). Through the observed data (satellite and climate reanalysis), we can observe a predominance of lower frequency of blocking events in years of SIE retraction, in relation to

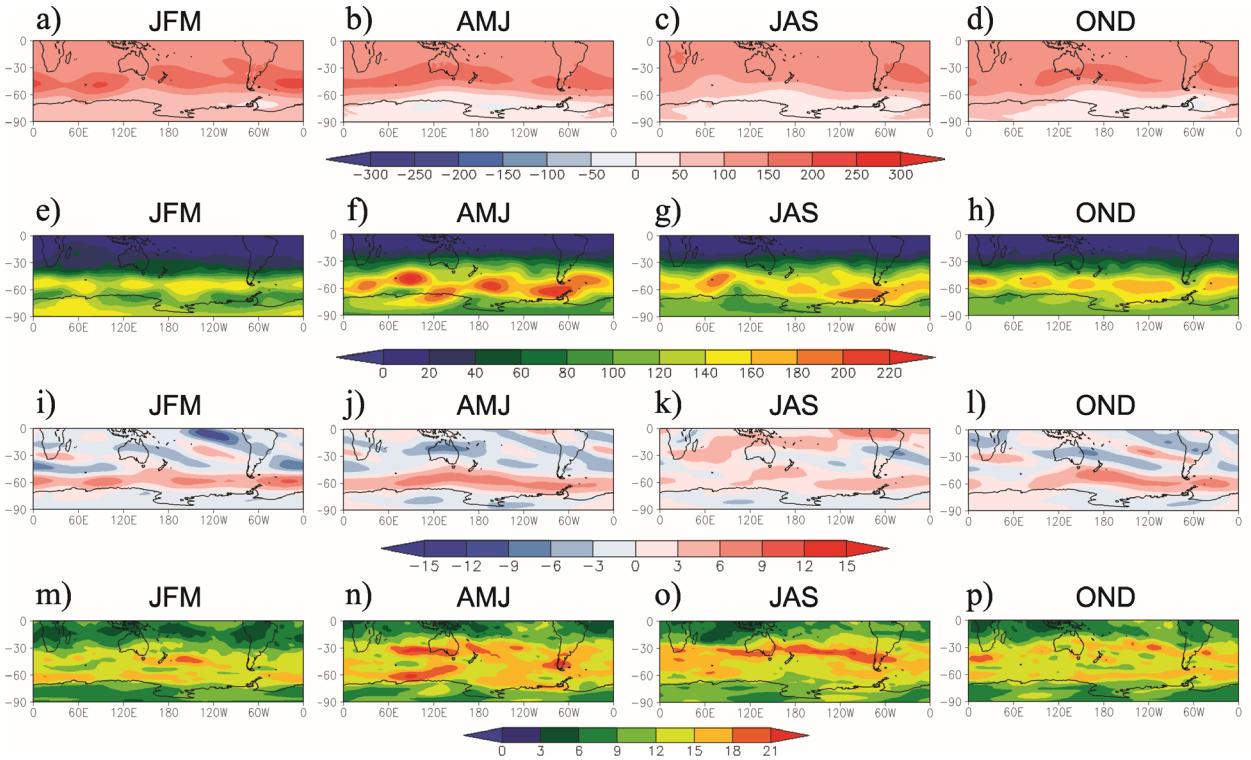

Figure 5. Seasonal difference of (a, b, c, d) 500-hPa geopotential height (m) and (i, j, k, l) 250-hPa zonal wind (ms^{-1}) between the CCSM4 historical experiment and the ERA-Interim reanalysis and standard deviation of (e, f, g, h) 500-hPa geopotential height (m) and (m, n, o, p) 250-hPa zonal wind (ms^{-1}) from the CCSM4 historical experiment during summer (JFM; first column), autumn (AMJ; second column), winter (JAS; third column) and spring (OND; fourth column) over 1979-2005.

years with expansion, in summer (exception of the Southeast and South Atlantic; Figure 8a) and winter (Figure 8c). In transition seasons there is an alternation between higher and lower frequency in years of SIE retraction (Figures 8b, 8d). In autumn, in years of SIE retraction, a higher frequency predominates in the eastern Indian Ocean, Southwest Pacific and South Atlantic, while a lower frequency dominates in the western Indian Ocean, Southeastern and central Pacific. In spring, in years of SIE retraction, a higher frequency predominates in the Indian Ocean and east-central Pacific, while a lower frequency predominates in the western Pacific and South Atlantic.

In MIROC5 (the model with the greatest Antarctic SIE underestimation) there is a lower frequency of blocking events in years of SIE retraction, compared to years with expansion, in summer (Southeast Pacific; Figure 8e), autumn (central-eastern South Pacific and South Atlantic; Figure 8f), winter (midwestern South Pacific and eastern Indian Ocean; Figure 8g) and spring (Southwestern and Southeastern Pacific; Figure 8h). On the other hand, a higher frequency prevails in years of SIE retraction in summer (midwestern South Pacific), autumn (Southwest Pacific and Indian Ocean), winter (Southeast Pacific and South Atlantic) and spring (Southeast Pacific).

In CCSM4 (model with the greatest Antarctic SIE overestimation) there is a lower frequency of blocking events in years of SIE retraction, in relation to years with expansion, in summer (Southeast and Central Pacific and South Atlantic; Figure 8i), autumn (center -western South Pacific; Figure 8j), winter (South Pacific; Figure 8k) and spring (Southeast Pacific; Figure 8l). On

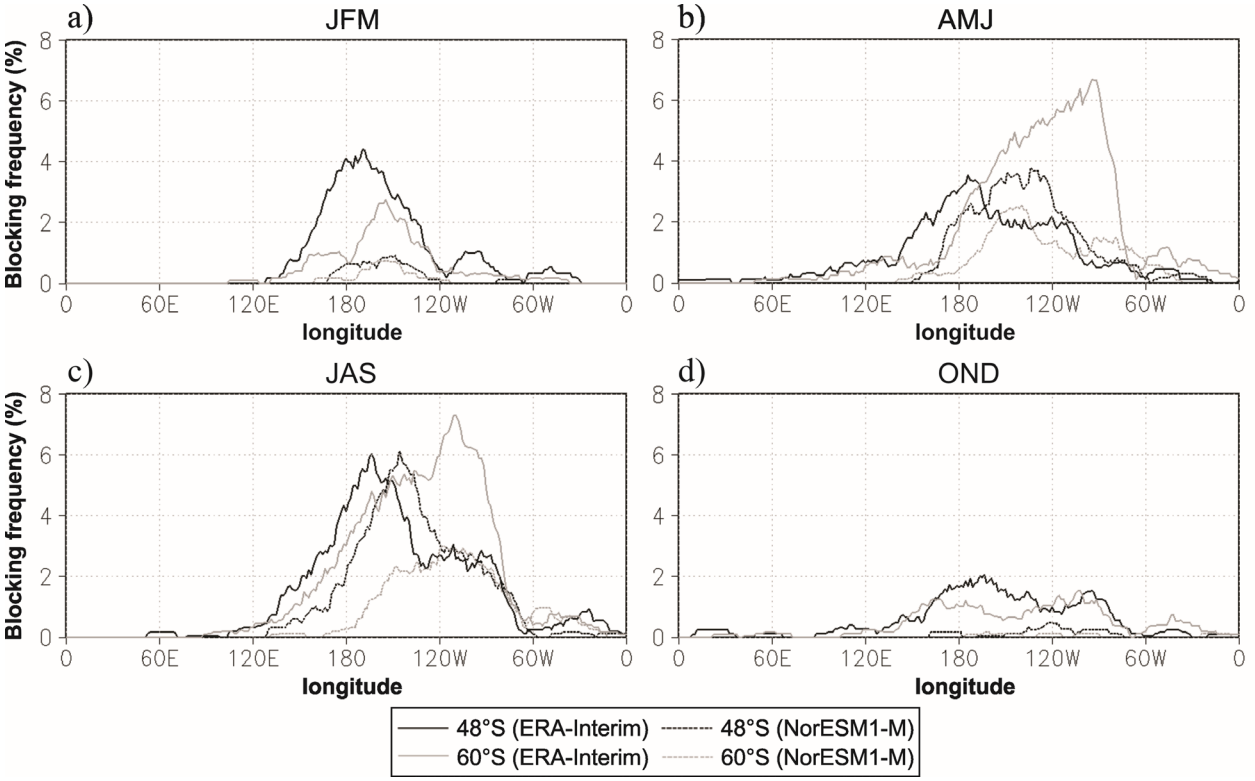

Figure 6. Seasonal frequency of blocking events by longitude (%) in the ERA-Interim reanalysis (continuous lines) and in the NorESM1-M historical experiment (dashed lines) during (a) summer (JFM), (b) autumn (AMJ), (c) winter (JAS) and (d) spring (OND) over 1979-2005.

the other hand, a higher frequency prevails in years of SIE retraction in summer (midwestern South Pacific), autumn (Southeast Pacific and South Atlantic), winter (Southeast Pacific) and spring (midwestern South Pacific).

In NorESM1-M (model with the best representation of the Antarctic SIE) there is a lower frequency of blocking event in years of SIE retraction, in relation to the years with expansion, in autumn (midwest of the South Pacific and South Atlantic; Figure 8n). On the other hand, a higher frequency prevails in years of SIE retraction in autumn (Southeast Pacific) and winter (South Pacific; Figure 8o).

Figure 9 shows the seasonal frequency of blocking events, in the 60°S latitude band, in years of SIE Antarctic retraction and expansion (1979-2005). Through the observed data (satellite and climate reanalysis), we can observe that there is a higher frequency in years of SIE retraction, in relation to years with expansion, in all seasons (Figures 9a-d). This increase is greatest in the South Pacific, being also observed in the Indian Ocean at all seasons and in the South Atlantic at transition seasons (Figures 9b, 9d).

Similarly, in MIROC5 (model with the greatest Antarctic SIE underestimation) the frequency of blocking events, in the 60°S latitude band, is predominantly higher in years of SIE retraction in all seasons (Figures 9e-h). The higher frequency is observed in the South Pacific (all seasons), in addition to the South Atlantic (between summer and winter) and the Indian Ocean (between autumn and spring).

In CCSM4 (the model with the greatest Antarctic SIE overestimation) the frequency of

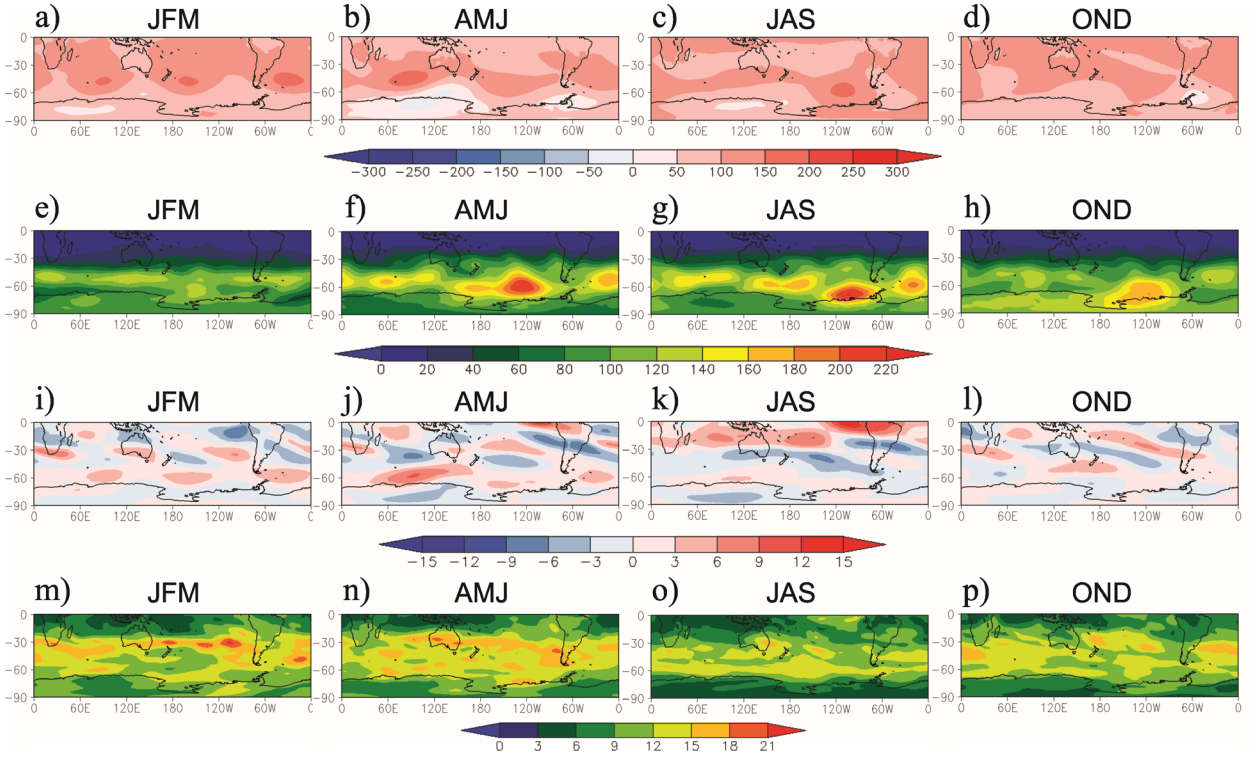

Figure 7. Seasonal difference of (a, b, c, d) 500-hPa geopotential height (m) and (i, j, k, l) 250-hPa zonal wind (ms^{-1}) between the NorESM1-M historical experiment and the ERA-Interim reanalysis and standard deviation of (e, f, g, h) 500-hPa geopotential height (m) and (m, n, o, p) 250-hPa zonal wind (ms^{-1}) from the NorESM1-M historical experiment during summer (JFM; first column), autumn (AMJ; second column), winter (JAS; third column) and spring (OND; fourth column) over 1979-2005.

blocking event in the Southern Hemisphere, in the 60°S latitude band, is also higher in years of SIE retraction in all seasons (Figures 9i-k) , with the exception of spring (Figure 9l). The higher frequency can be seen in the midwestern South Pacific (summer), South Pacific (autumn), Southeast Pacific (winter) and South Atlantic (summer, autumn and winter). On the other hand, a higher frequency prevails in years of SIE expansion in spring, observed in the South Pacific.

In NorESM1-M (model with the best representation of the Antarctic SIE) the frequency of blocking events, in the 60°S latitude band, is predominantly higher in years of SIE retraction in all seasons (Figures 9n-p), except of summer (Figure 9m). The higher frequency occurs in the midwestern South Pacific (autumn), South Pacific (winter and spring) and South Atlantic (winter and spring). On the other hand, a higher frequency prevails in years of SIE expansion in the summer, observed in the South Pacific.

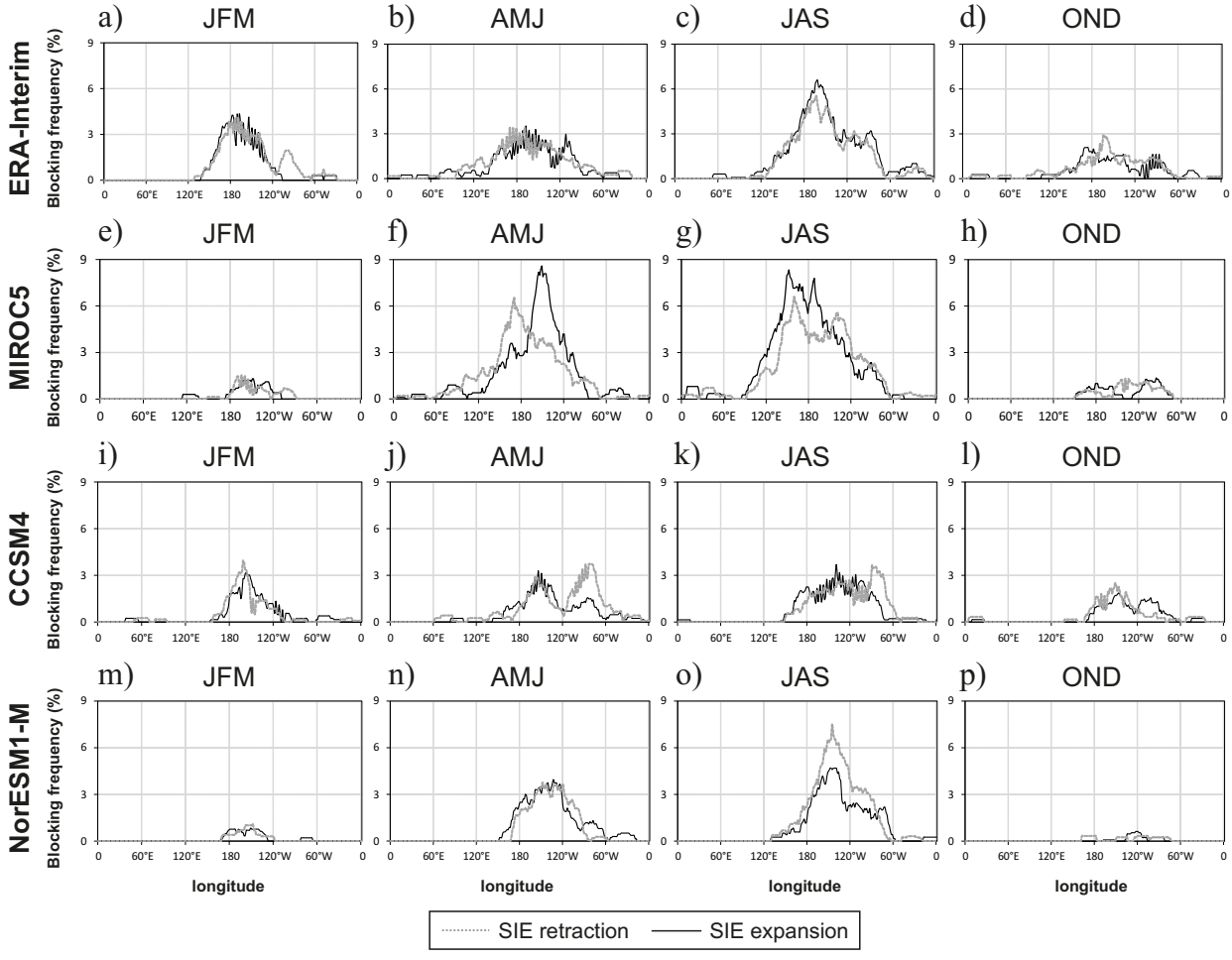

Figure 8. Seasonal frequency of blocking events, in the 48°S latitude band, in years of SIE Antarctic retraction (gray line) and expansion (black line) for (a, b, c, d) observed data (satellite and reanalyses), (e, f, g, h) MIROC5, (i, j, k, l) CCSM4 and (m, n, o, p) NorESM1-M during summer (JFM; first column), autumn (AMJ; second column), winter (JAS; third column) and spring (OND; fourth column) over 1979-2005.

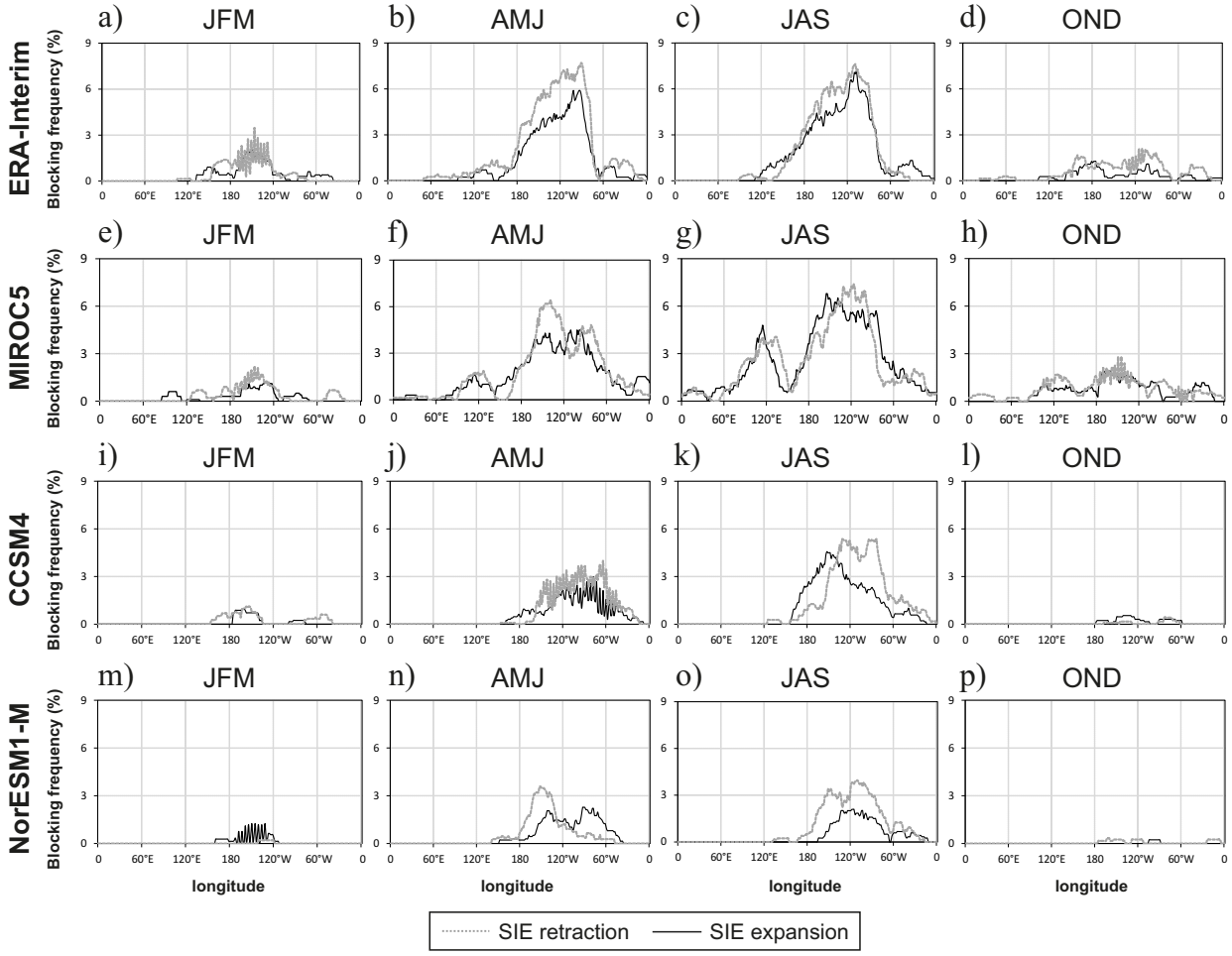

Figure 9. Seasonal frequency of blocking events, in the 60°S latitude band, in years of SIE Antarctic retraction (gray line) and expansion (black line) for (a, b, c, d) observed data (satellite and reanalyses), (e, f, g, h) MIROC5, (i, j, k, l) CCSM4 and (m, n, o, p) NorESM1-M during summer (JFM; first column), autumn (AMJ; second column), winter (JAS; third column) and spring (OND; fourth column) over 1979-2005.

DISCUSSION AND CONCLUSIONS

This study investigated whether there are differences in the frequency and position of Southern Hemisphere atmospheric blockings between CMIP5 models (MIROC5, NorESM1-M and CCSM4) with different representations of Antarctic SIE in historical experiments over 1979-2005. In the AOGCM with the highest underestimation of the Antarctic SIE, MIROC5, there are atmospheric conditions favorable to the occurrence of atmospheric blockings, with a predominance of overestimation in the simulated frequency of blocking events, especially in autumn and winter, in relation to the ERA-Interim reanalysis. On the other hand, in the AOGCM with the highest overestimation of the Antarctic SIE, CCSM4, atmospheric conditions are unfavorable to the occurrence of atmospheric blockings, with an underestimation in the simulated frequency of blocking events in all seasons. The same is observed in the model with the best representation of the Antarctic SIE, NorESM1-M, which overestimates the SIE, showing a predominance of underestimation of the simulated frequency of blocking events in all seasons and latitude bands.

In the model with the highest underestimation of the Antarctic SIE (MIROC5), we observed a weakening of the polar jet and an increase in the 500-hPa geopotential height, more intense to south of 40-50°S, in relation to the climate reanalysis. This possibly occurs, because a lower SIE results in a reduction in surface albedo and a consequent increase in the absorption of solar radiation, which results in an increase in the ocean surface temperature and in the heat flows from the ocean to the atmosphere, heating the adjacent atmosphere (Menéndez et al. 1999, Cunningham & Bonatti 2011). Warm air is lighter than cold air, thus the pressure surfaces rises, which can be evidenced by the more intense increase of the 500-hPa geopotential height to the south of 40-50°S, reducing the meridional pressure gradients between the mid- and high latitudes of the Southern Hemisphere. In this way, the westerly winds and the polar jet around the Antarctic continent are weakened, this has also been observed in previous studies through numerical experiments (Raphael et al. 2011, Parise et al. 2015). The weakening of the zonal flow tends to favor the amplification of the ridges and troughs, which contribute to the occurrence of atmospheric blockings (Liu et al. 2012), observed through the overestimation of the frequency of blocking events by the MIROC5.

On the other hand, we can observe the relatively opposite pattern in the model with the highest overestimation of the Antarctic SIE (CCSM4). The polar jet is more intense, as is the 500-hPa geopotential height, although the latter has weaker positive differences in the Antarctic region, reaching negative differences in autumn and winter. A higher SIE results in an increase in albedo and a reduction for radiation absorbed by the surface. In this way, there is a reduction in the ocean surface temperature and in the heat flows between the ocean and the atmosphere, contributing to the cooling of the adjacent atmosphere (Menéndez et al. 1999, Cunningham & Bonatti 2011) and the lowering of the pressure surfaces, evident through the weak positive or negative differences in the 500-hPa geopotential height in the Antarctic region. Thus, the meridional pressure gradients between the mid- and high latitudes increase, strengthening the zonal flow around the Antarctic continent, demonstrated by the strengthening of the polar jet. With the zonal flow strengthened, the southern flow is hampered, making it difficult to form atmospheric blockings, as observed by the frequency of blocking events underestimation in the CCSM4 simulations.

A pattern similar to CCSM4 is observed in the AOGCM with better representation of the Antarctic SIE (NorESM1-M), since this model is largely based on CCSM4 (Bentsen et al. 2013), also presenting an overestimation of the Antarctic SIE.

All models present a good representation of the preferred atmospheric blocking regions in the Southern Hemisphere over the South Pacific, although they do not represent the longitudinal location of the maximum frequency. The assessment of atmospheric blockings in climate models depends on the bias in the representation of the basic state (Scaife et al. 2010) or the variability (Barriopedro et al. 2010, Vial & Osborn 2012). The observed variability of the 500-hPa geopotential height and 250-hPa zonal wind, in the MIROC5, CCSM4 and NorESM1-M, is greater especially in the cold seasons and over the South Pacific, alternatively, in the seasons and in the region with the highest frequency of atmospheric blockings (Van Loon 1956, Tibaldi et al. 1994, Lejeñas 1984, Trenberth & Mo 1985, Oliveira & Ambrizzi 2016).

In the 60°S latitude band, there is a predominance of a higher frequency of blocking events in the Southern Hemisphere, for all models and observed data (satellite and climate

reanalysis) in years of SIE retraction. On the other hand, the frequency is lower in years of SIE expansion. In the 48°S latitude band, there is an alternation between lower and higher frequency of blocking events in the Southern Hemisphere in years of SIE retraction and expansion. Thus, there is no evident spatial pattern in the frequency of blocking events associated with the Antarctic SIE retraction and expansion in the 48°S latitude band. These results support the fact that the model with the greatest Antarctic SIE underestimation (MIROC5) has a higher frequency of blocking events, while the model with the greatest Antarctic SIE overestimation (CCSM4) has a lower frequency.

In recent years, the Antarctic SIE has shown an abrupt reduction (Parkinson 2019). If this condition persists in the coming years, there may be a favorable effect on the occurrence of the Southern Hemisphere atmospheric blockings, which are associated with extreme weather events. Thus, the results of this study present potential forerunners for mid- and long-term forecasting of the Southern Hemisphere atmospheric blockings. In addition, these will contribute to the understanding of the mechanisms related to atmospheric blockings, assisting in the implementation of more appropriate representations of the general atmospheric circulation in large-scale models, increasing forecasting abilities.

Acknowledgments

CBC was supported by the Fundação de Amparo à Pesquisa do Estado de São Paulo (FAPESP) under Grant 2012/17370-2, and by the Instituto Nacional de Ciência e Tecnologia da Criosfera (Conselho Nacional de Desenvolvimento Científico e Tecnológico – CNPq – Research Grant 465680/2014-3). TA was supported by the Instituto Nacional de Ciência e Tecnologia para Mudanças Climáticas fase 2 under CNPq Grant 465501/2014-1, FAPESP Grants 2014/50848-9 and 2017/09659-6; and partially funded by CNPq Grants 304298/2014-0 and 420262/2018-0. We are grateful for the constructive feedback provided by the reviewers.

REFERENCES

AMBRIZZI T, MARQUES R & NASCIMENTO E. 2009. Bloqueios atmosféricos. In: CAVALCANTI ET AL. (Org), Tempo e Clima no Brasil. 1st ed., São Paulo: Oficina de Textos, p. 279-296.

BARRIOPEDRO D, GARCÍA-HERRERA R, GONZÁLEZ-ROUCO JF & TRIGO RM. 2010. Application of blocking diagnosis methods to General Circulation Models. Part II: model simulations. Clim Dynam 35: 1393-1409.

BARRIOPEDRO D, GARCÍA-HERRERA R, LUPO AR & HERNÁNDEZ E. 2006. A climatology of Northern Hemisphere blocking. J Climate 19: 1042-1063.

BATES GT & MEEHL GA. 1986. The effect of co2 concentration on the frequency of blocking in a general-circulation model coupled to a simple mixed layer ocean model. Mon Weather Rev 114: 687-701.

BENTSEN M ET AL. 2013. The Norwegian Earth System Model, NorESM1-M - Part 1: Description and basic evaluation of the physical climate. Geosci Model Dev 6: 687-720.

COUGHLAN MJ. 1983. A comparative climatology of blocking action in the two hemispheres. Aust Meteorol Mag 31(01): 3-13.

CUNNINGHAM CA & BONATTI JP. 2011. Local and remote responses to opposite Ross Sea ice anomalies: a numerical experiment with the CPTEC/INPE AGCM. Theor Appl Climatol 106: 23-44.

DOLE RM. 1986a. Persistent anomalies of the extratropical Northern Hemisphere wintertime circulation: Structure. Mon Weather Rev 114: 178-207.

DOLE RM. 1986b. The life cycles of persistent anomalies and blocking over the North Pacific. Adv Geophys 29: 31-69.

ESCOBAR G. 2009. Weather and climate in Brazil. High-level jets. 1st. ed, São Paulo: Oficina de Textos, 463 p.

GENT PR ET AL. 2011. The Community Climate System Model Version 4. J Climate 24: 4973-4991.

HIGGINS RW & SCHUBERT SD. 1994. Simulated life cycles of persistent anticyclonic anomalies over the North Pacific: Role of synoptic-scale eddies. J Atmos Sci 51: 3238-3259.

HIGGINS RW & SCHUBERT SD. 1996. Simulations of persistent North Pacific circulation anomalies and interhemispheric teleconnections. J Atmos Sci 53: 188-207.

IPCC. 2013. Climate Change 2013: The Physical Science Basis. Contribution of Working Group I to the Fifth Assessment Report of the Intergovernmental Panel on Climate Change. In: Stocker TF, Qin D, Plattner G-K, Tignor M, Allen SK, Boschung J, Nauels A, Xia Y, Bex V & Midgley

PM (Eds), Cambridge University Press, Cambridge, United Kingdom and New York, NY, USA, 1535 p.

KALKSTEIN LS, JAMASON PF, GREENE JS, LIBBY J & ROBINSON L. 1996. The Philadelphia hot weather-health watch/warning system: Development and application, summer 1995. Bull Amer Meteor Soc 77: 1519-1528.

KARL TR & KNIGHT RW. 1997. The 1995 Chicago heat wave: How likely is a recurrence? Bull Amer Meteor Soc 78: 1107-1119.

KIDSTON J, TASCHETTO AS, THOMPSON DWJ & ENGLAND MH. 2011. The influence of Southern Hemisphere sea-ice extent on the latitude of the mid-latitude jet stream. Geophys Res Lett 38: L15804.

KIKUCHI Y. 1969. Numerical simulation of the blocking process. J Met Soc Japan 47: 29-54.

KOLDUNOV NV, STAMMER D & MAROTZKE J. 2010. Present-day Arctic sea ice variability in the coupled ECHAM5/MPI-OM model. J Climate 23: 2520-2543.

LANDRUM L, HOLLAND MM, SCHNEIDER DP & HUNKE E. 2012. Antarctic sea ice climatology, variability, and late twentieth-century change in CCSM4. J Climate 25: 4817-4838.

LEJENÃS H. 1984. Characteristics of Southern Hemisphere Blocking as determined from a time series of observational data. Q J Roy Meteor Soc 110: 967-979.

LIU J, CURRY JA, WANG H, SONG M & HORTON RM. 2012. Impact of declining Arctic sea ice on winter snowfall. P Natl Acad Sci 109: 4074-4079.

LUO D, CHEN X, DAI A & SIMMONDS I. 2018. Changes in Atmospheric Blocking Circulations Linked with Winter Arctic Warming: A New Perspective. J Climate 31(18): 7661-7678.

LUO D, LI J & HUANG F. 2002. Life Cycles of Blocking Flows Associated with Synoptic-scale Eddies: Observed Results and Numerical Experiments. Adv Atmos Sci 19: 594-618.

LUPO AR & SMITH PJ. 1998. The interactions between a midlatitude blocking anticyclone and synoptic-scale cyclones that occurred during the summer season. Mon Wea Rev 126: 502-515.

MARQUES RFC & RAO VB. 1999. A diagnosis of a long lasting blocking event over the southeast Pacific Ocean. Mon Wea Rev 127: 1761-1776.

MELSOM A, LIEN V & BUDGELL WP. 2009. Using the Regional Ocean Modeling System (ROMS) to improve the ocean circulation from a GCM 20th century simulation. Ocean Dyn 59: 969-981.

MENDES MCD, TRIGO RM, CAVALCANTI IFA & CAMARA CC. 2008. Blocking Episodes in the Southern Hemisphere: Impact on the Climate of Adjacent Continental Areas. Pure Appl Geophys 165: 1941-1962.

MENÉNDEZ CG, SERAFINI YV & LE TREUT H. 1999. The storm tracks and the energy cycle of the Southern Hemisphere: sensitivity to sea-ice boundary conditions. Ann Geophys 17: 1478-1492.

MO KC, NOGUES PEAGLE J & HIGGINS RW. 1997. Atmospheric processes associated with summer floods and droughts in the central United States. J Climate 10: 3028-3046.

NAKAMURA H. 1994. Rotational evolution of potential vorticity associated with a strong blocking flow configuration over Europe. Geophys Res Lett 21: 2003-2006.

NAKAMURA H & FUKAMACHI T. 2001. Evolution and Dynamics of Summertime Blocking over the Far East and Associated Surface Okhotsk High. Quart J Roy Meteorol Soc 130: 1213-1233.

NAKAMURA H, NAKAMURA M & ANDERSON JL. 1997. The Role of High- and Low-frequency Dynamics in Blocking Formation. Mon Wea Rev 125: 2074-2093.

NAKAMURA H & WALLACE M. 1993. Synoptic behavior of baroclinic eddies during the blocking onset. Mon Wea Rev 121: 1892-1903.

OLIVEIRA FNM & AMBRIZZI T. 2016. The effects of ENSO-types and SAM on the large-scale southern blockings. Int J Climatol 37: 3067-3081.

OLIVEIRA FNM, CARVALHO LMV & AMBRIZZI T. 2014. A new climatology for Southern Hemisphere blockings in the winter and the combined effect of ENSO and AAO phases. Int J Climatol 34: 1676-1692.

PARISE CK, PEZZI LP, HODGES KI & JUSTINO F. 2015. The Influence of Sea Ice Dynamics on the Climate Sensitivity and Memory to Increased Antarctic Sea Ice. J Climate 28: 9642-9668.

PARKINSON CL. 2019. A 40-y record reveals gradual Antarctic sea ice increases followed by decreases at rates far exceeding the rates seen in the Arctic. P Natl Acad Sci USA 116(29): 14414-14423.

POLVANI LM & SMITH KL. 2013. Can natural variability explain observed Antarctic sea ice trends? New modeling evidence from CMIP5. Geophys Res Lett 40(12): 3195-3199.

RAPHAEL MN, HOBBS W & WAINER I. 2011. The effect of Antarctic sea ice on the Southern Hemisphere atmosphere during the southern summer. Clim Dynam 36: 1403-1417.

REX DF. 1950. Blocking Action in the Middle Troposphere and Its Effect upon Regional Climate. Tellus 2(4): 275-301.

RODRIGUES RR & WOOLLINGS T. 2017. Impact of Atmospheric Blocking on South America in Austral Summer. J Climate 30: 1821-1837.

ROSENBLUM E & EISENMAN I. 2017. Sea Ice Trends in Climate Models Only Accurate in Runs with Biased Global Warming. J Climate 30(16): 6265-6278.

SCAIFE AA, WOOLLINGS T, KNIGHT J, MARTIN G & HINTON T. 2010. Atmospheric blocking and mean biases in climate models. J Climate 23: 6143-6152.

SHABBAR A, HUANG J & HIGUCHI K. 2001. The relationship between the wintertime North Atlantic Oscillation and blocking episodes in the North Atlantic. Int J Climatol 21(3): 355-369.

SHUKLA J. 1986. SST anomalies and blocking. Adv Geophys 29: 443-452.

SINCLAIR MR. 1996. A climatology of anticyclones and blocking for the Southern Hemisphere. Mon Weather Rev 124: 245-263.

TANG Q, ZHANG X, YANG X & FRANCIS JA. 2013. Cold winter extremes in northern continents linked to Arctic sea ice loss. Environ Res Lett 8: 1-6.

TAYLOR KE, STOUFFER RJ & MEEHL GA. 2012. An Overview of CMIP5 and the experiment design. Bull Amer Meteor Soc 93: 485-498.

THORNDIKE AS, ROTHROCK DA, MAYKUT GA & COLONY R. 1975. The thickness distribution of sea ice. J Geophys Res 80: 4501-4513.

TIBALDI S, D'ANDREA F, TOSI E & ROECKNER E. 1997. Climatology of Northern Hemisphere blocking in the ECHAM model. Clim Dynam 13: 649-666.

TIBALDI S, TOSI E, NAVARRA A & PEDULLI L. 1994. Northern and Southern Hemisphere variability of blocking frequency and predictabilty. Mon Weather Rev 122: 1971-2003.

TRENBERTH KE. 1991. Storm track in the Southern Hemisphere. J Atmos Sci 48: 2159-2178.

TRENBERTH KE & GUILLEMOT CJ. 1995. Evaluation of the global atmospheric moisture budget as seen from analyses. J Climate 8: 2255-2280.

TRENBERTH KE & MO K. 1985. Blocking in the Southern Hemisphere. Mon Weather Rev 113: 2-21.

TSOU CH & SMITH PJ. 1990. The role of synoptic/planetary-scale interactions during the development of a blocking anticyclone. Tellus 42: 174-193.

TURNER J, BRACEGIRDLE TJ, PHILLIPS T, MARSHALL GJ & HOSKING JS. 2013. An Initial Assessment of Antarctic Sea Ice Extent in the CMIP5 Models. J Climate 26: 1473-1484.

TYRLIS E & HOSKINS BJ. 2008. Aspects of a Northern Hemisphere Atmospheric Blocking Climatology. J Atmos Sci 65: 1638-1652.

VAN LOON H. 1956. Blocking Action in the Southern Hemisphere - Part I. Notos 5: 171-175.

VERDECCHIA MG, VISCONTI F, D'ANDREA F & TIBALDI S. 1996. A neural network approach for blocking recognition. Geophys Res Lett 23: 2081-2084.

VIAL J & OSBORN TJ. 2012. Assessment of atmosphere–oceangeneral circulation model simulations of winter NorthernHemisphere atmospheric blocking. Clim Dynam 39: 95-112.

WASHINGTON WM & MEEHL GA. 1984. Seasonal cycle experiments on the c1imate sensitivity due to a doubling of CO2 with an atmospheric general circulation model coupled to a sim pie mixed layer ocean model. J Geophys Res 89: 9475-9503.

WATANABE M ET AL. 2010 Improved Climate Simulation by MIROC5: Mean States, Variability, and Climate Sensitivity. J Climate 23: 6312-6335.

ZUNZ V, GOOSSE V & MASSONNET F. 2013. How does internal variability influence the ability of CMIP5 models to reproduce the recent trend in Southern Ocean sea ice extent? Cryosphere 7(2): 451-468.

ZWALLY HJ, COMISO JC, PARKINSON CL, CAVALIERI DJ & GLOERSEN P. 2002. Variability of Antarctic sea ice 1979-1998. J Geophys Res 107.

How to cite

CARPENEDO CB & AMBRIZZI T. 2022. Atmospheric blockings in Coupled Model Intercomparison Project Phase 5 models with different representations of Antarctic sea ice extent. An Acad Bras Cienc 94: e20210432. DOI 10.1590/0001-3765202220210432.

Manuscript received on March 25, 2021;
accepted for publication on August 21, 2021

CAMILA B. CARPENEDO[1]
https://orcid.org/0000-0001-9034-789X

TÉRCIO AMBRIZZI[2]
https://orcid.org/0000-0001-8796-7326

[1]Universidade Federal do Paraná, Setor de Ciências Agrárias, Departamento de Solos e Engenharia Agrícola, Rua dos Funcionários, 1540, Cabral, 80035-050 Curitiba, PR, Brazil

[2]Universidade de São Paulo, Instituto de Astronomia, Geofísica e Ciências Atmosféricas, Departamento de Ciências Atmosféricas, Rua do Matão, 1226, Cidade Universitária, 05508-090 São Paulo, SP, Brazil

Correspondence to: **Camila B. Carpenedo**
E-mail: camila.carpenedo@ufpr.br

Author contributions

Conceptualization, CBC, and TA; Methodology, CBC; Data curation, CBC; Original draft preparation, CBC; Formal analysis, CBC, and TA; Reviewing and editing, CBC, and TA.